Technical University of Denmark

DTU

LES tests on airfoil trailing edge serration

Zhu, Wei Jun; Shen, Wen Zhong

Link back to DTU Orbit

DTU Library
Technical Information Center of Denmark

You may also be interested in:

LES tests on airfoil trailing edge serration

Wei Jun Zhu[1,2], Wen Zhong Shen[2]

[1] Yangzhou University, Yangzhou, China
[2] Technical University of Denmark, Lyngby 2800, Denmark

Email: wjzh@dtu.dk

Abstract. In the present study, a large number of acoustic simulations are carried out for a low noise airfoil with different Trailing Edge Serrations (TES). The Ffowcs Williams-Hawkings (FWH) acoustic analogy is used for noise prediction at trailing edge. The acoustic solver is running on the platform of our in-house incompressible flow solver EllipSys3D. The flow solution is first obtained from the Large Eddy Simulation (LES), the acoustic part is then carried out based on the instantaneous hydrodynamic pressure and velocity field. To obtain the time history data of sound pressure, the flow quantities are integrated around the airfoil surface through the FWH approach. For all the simulations, the chord based Reynolds number is around 1.5×10^6. In the test matrix, the effects from angle of attack, the TE flap angle, the length/width of the TES are investigated. Even though the airfoil under investigation is already optimized for low noise emission, most numerical simulations and wind tunnel experiments show that the noise level is further decreased by adding the TES device.

1. Objectives

To further reduce wind turbine aerodynamically generated noise, smart design at blade trailing edge (TE) using active or passive flow control become popular choices to control the total dB level. Active flow control, such as wall suction [1] has shown positive effect on the TE noise reduction by decreasing the boundary layer thickness at TE. Other active control, such as flow blowing flap [2], is demonstrated that the blowing greatly weakens the vortex system and deceases noise generation. As a feasible technique, passive flow control methods for wind turbine blades are more practical. For example, the passive devices at TE can be either brushes [3, 4] and serrations [5, 6, 7, 8, 9] or even porous serrations [10]. The TE brushes and serrations for wind turbine applications are still under investigation. Physical understanding of flow mechanisms around serrations is needed in order to carry out detailed design work. The identification of the flow mechanisms by which the airfoil noise reduction is achieved is an important task. Based on the works of bionic structure of the owl [10, 11], some significant applications to develop silent airframes [12], wind turbine rotors [9] and many other aerodynamic structures [13] are successfully achieved.

The aim of the current work is to numerically investigate the effect of TES. Quite many previous achievements on serrated airfoil investigations were carried out experimentally. Despite the truth that noise reduction of each airfoil and rotor blade is achieved, the differences of experimental observations exist. Based on different experimental conditions, such as Reynolds number and flow

angle of attack, the reduction of airfoil noise seems to be a function of frequency. On the modelling side, it is expected that advanced computational aero-acoustic methods can provide more accurate prediction of noise from a serrated trailing edge. So far, the parametric trends of airfoil noise reduction using various serration geometries require more research on this topic. In order to find some general trend from TES, a large number of LES/FWH simulations are carried out in the present research.

2. Numerical methods

In this work, the integrated formulation proposed by Farassat [14] is applied. The formulation is the solution of the FW-H equation with surface sources only when the surface moves at subsonic speed. This formulation has been successfully used for helicopter rotor and propeller noise predictions. At the retarded or emission time, the thickness and loading noise equations are written as

$$4\pi p'_T (\vec{x},t) = \frac{\partial}{\partial t} \int_{f=0} \left[\frac{\rho_0 v_n}{r(1-M_r)} \right]_{res} dS \tag{1}$$

$$4\pi p'_L (\vec{x},t) = \frac{1}{c} \frac{\partial}{\partial t} \int_{f=0} \left[\frac{p\cos\theta}{r(1-M_r)} \right]_{res} dS + \int_{f=0} \left[\frac{p\cos\theta}{r^2(1-M_r)} \right]_{res} dS \tag{2}$$

The right hand sides of Eqs. (1) and (2) are the integrations of time history variables obtained from flow calculations. The variables include wall normal velocity v_n, the Mach number of the source in the radiation direction M_r, the pressure on the solid wall surface p, the distance between source and receiver r, the angle between radiation direction and the local wall normal direction θ. The acoustic solver may run in parallel with flow model, in practice the acoustic solver starts when the flow-field is fully established. The necessary time history flow data are recoded in advance in order to calculate the time derivatives at emission time.

For the flow simulations, the filtered incompressible equations are solved by the in-house EllipSys3D code [15, 16]. The momentum, turbulent stresses and eddy viscosity equations are applied to obtain the flow data.

$$\frac{\partial \overline{U}_i}{\partial t} + \frac{\partial \left(\overline{U}_i \overline{U}_j \right)}{\partial x_j} = -\frac{1}{\rho} \frac{\partial \overline{P}}{\partial x_i} + \nu \frac{\partial^2 \overline{U}_i}{\partial x_j^2} + \frac{\partial \tau_{ij}}{\partial x_j} \tag{3}$$

$$\tau_{ij} = \nu_t \left(\frac{\partial \overline{U}_i}{\partial x_j} + \frac{\partial \overline{U}_j}{\partial x_i} \right) - \frac{2}{3} k \delta_{ij} \tag{4}$$

$$\nu_t = C \left| \overline{\vec{\omega}} \right|^\alpha k^{(1-\alpha)/2} \Delta^{(1+\alpha)} \tag{5}$$

In Eqs. (3) and (4), the first filter is identified by a bar (¯) which is due to the finest mesh. The turbulent stresses τ_{ij} defined in Eq. (4) are modelled with an eddy viscosity. The eddy viscosity is then calculated by a mixed scale model where $\vec{\omega}$ is vorticity, $\Delta = \left(\Delta_x \Delta_y \Delta_z \right)^{1/3}$ is an average grid size, C is the model constant and $\alpha = 0.5$.

3. LES/Acoustic tests and validations

The airfoil geometry and the flow conditions are set according to the experiments:

1. Airfoil: CQU-DTU-LN118 airfoil, chord=0.6m, span=1.8m (0.6m effective span is used for noise integration).

2. Angles of Attack: 0, 4 and 8 degrees.

3. Wind Speed=45 m/s. Sound speed=344 m/s.

The airfoil under investigation is the in-house designed low noise airfoil with 18% relative thickness. The microphone array has a focus region such that the noise signal is collected along a span of 0.6m. According to the measurements, similar procedure is carried out during LES simulation where acoustic integration is applied in same region over the suction wall surface. LES simulations were conducted at a wind speed of 45m/s and angles of attack of 0,4 and 8 degrees.

The variables that are included in the test matrix are shown in Table 1 where α is the flow angle of attack, β is the flap angle of the TES, L/c is the normalized amplitude (length) of TES, λ/L is the aspect ratio between the wavelength (width) and the amplitude. By taking into account all the parameters, the total number of simulation will be 81 which is quite time consuming. To reduce the computational effort, the λ/L configuration is only considered for the cases of L/c=21%, β=0º and α=0 º, 4 º, 8º. Therefore the computational matrix consists of 39 simulations in total, including simulations of the baseline airfoil.

α (o)	0	4	8
β (o)	-5	0	5
L/c	7%	14%	21%
λ/L	0.25	0.5	1

Table 1: The test parameters.

Time history data are recorded at 11 locations near the TE. As shown in Figure 1 (a), there are 9 locations distributed along the airfoil span at the chord-wise location of x/c=98%, there are two more points located at x/c=102% and 106%. At each of the test location, velocity and pressure data are saved for 64 points which are distributed in the wall normal direction. The corresponding sound pressure level is seen in Figure 2 for angle of attack 0º, 4º and 8º degrees. The noise level is seen increased while angle of attack increases. Noise reduction is found from most of the simulations with the TES.

(a)

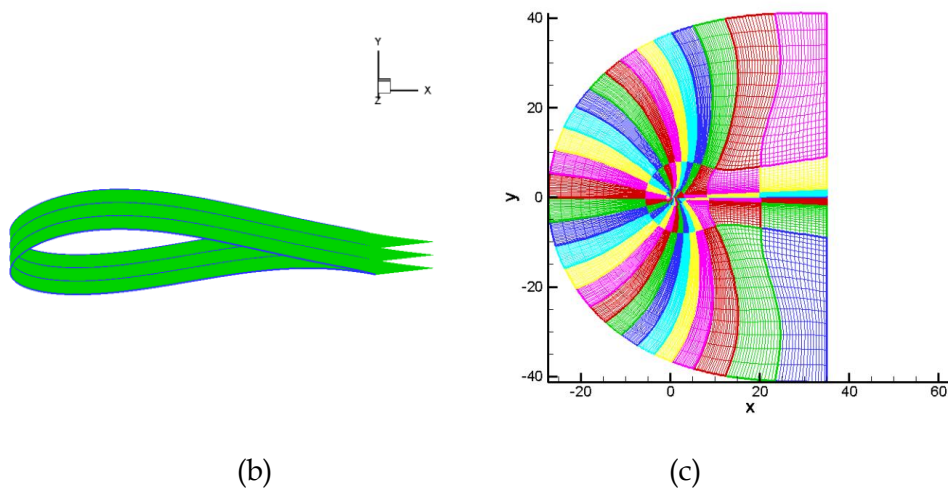(b)   (c)
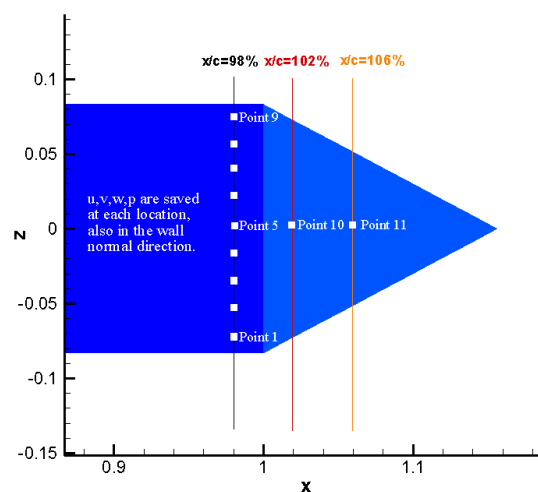
Fig. 1. (a) The locations of the test points; (b) Wall surface mesh; (c) Mesh side view.

At each of the test location, velocity and pressure data are saved for 64 points which are distributed in the wall normal direction. An example of the recorded velocity signal is shown in Figure 2. The simulation is started at time zero and stabilized after some iteration. From data1 to data16, the velocity gradually increase as the off-wall distance becomes larger. The full geometry of the TES is shown in Figure 3. The first three rows are the combination of TES flap angle and the amplitude (the root to tip length of the TES), the last row shows the aspect ratio between the wavelength and amplitude. For these 12 cases, three flow angles of attack are considered, that is in total 12x3 simulations.
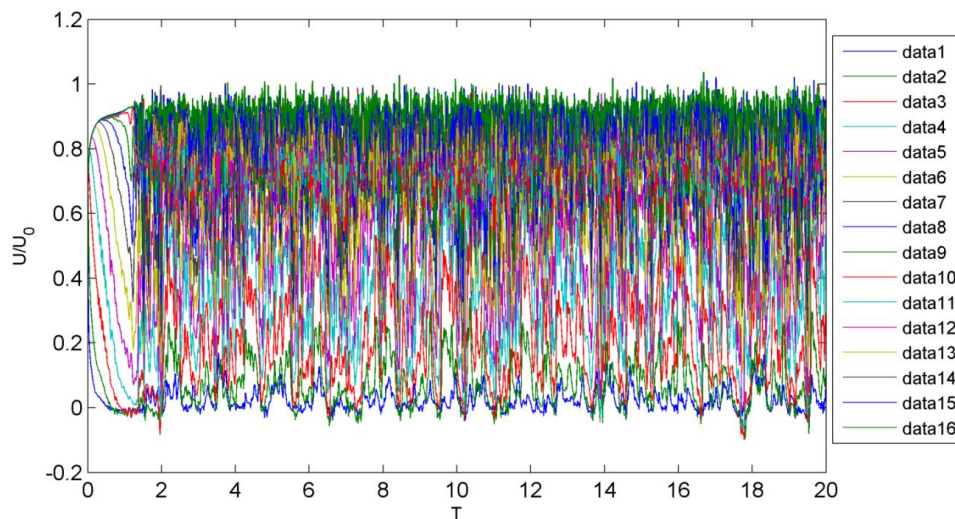

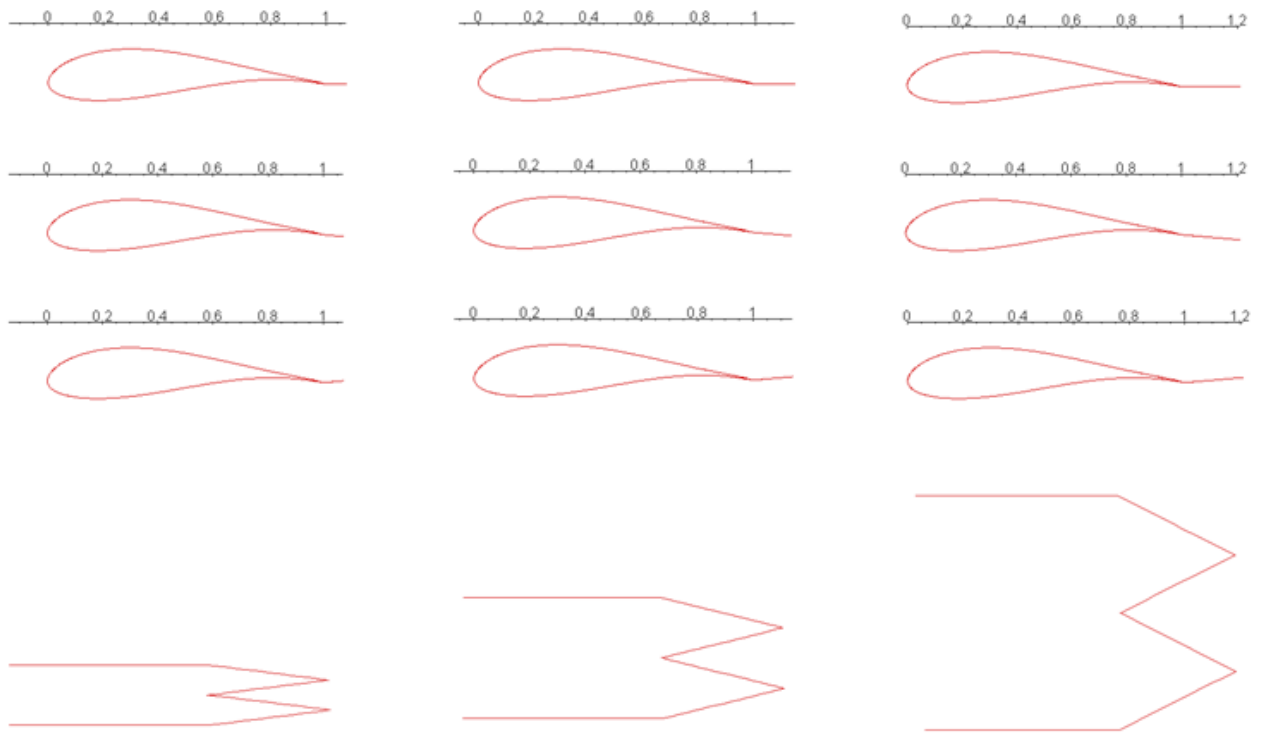Fig. 2. Example of the time history velocity along wall normal direction.

Fig. 3. The full picture of all the TES test matrix.

For each LES simulation, time history data (pressure and three velocity components) are saved at 11 test positions (see Fig. 1). Each position contains 64 points along wall normal direction to record the boundary layer information. Simulations are repeated for 39 times according to the parameter changes (Table 1).

As shown in Figure 1(b) and (c) a C-type 3D volume mesh is created based on the wall surface mesh. According to the earlier works [17, 18], the mesh resolution in terms of wall units shall be small and satisfy certain cell aspect ratio limitations. In the present case, the first wall cell size Δy is in the order of 10^{-5} chords and the ratio of $\Delta x/\Delta y$ is around 25 along the airfoil wall surface with Δx indicates grid size in the flow direction. Periodic flow condition is assumed at the two ends. The total number of blocks is 200 for the meshes with one serration.

For the current LES simulations of TES, the computational efficiency has been considered as an important factor. It is expected that the use of a large span size with more serrations represents flow-field better than using a narrow span. It is often a practical issue of choosing resonable span size, which is typically limitted by the avialable computer resources. The left plot in Fig. 4 shows the Cp results computed with *SpanA* and *SpanB* where *SpanA* contains 3 serrations and *SpanB* contains 1 serration. The difference between the two curves is hardly seen from the plot that indicates flow three-dimensionality is not playing an important role at this angle of attack. However, attention should be paid at very large angles of attack where three dimentional effect can be more significant. On the right plot in Fig. 4, the Cp values are compared at two spanwise locations: the values cut through serration tip (*SliceA*) and through serration root (*SliceB*). As it can be seen that *SliceA* has an extended area at trailing edge which is due to the contribution from the serration. As observed from the comparion,

some small deviation does exist near the traling edge, which only makes little change in flow-field but is enough to generate noise at different levels.
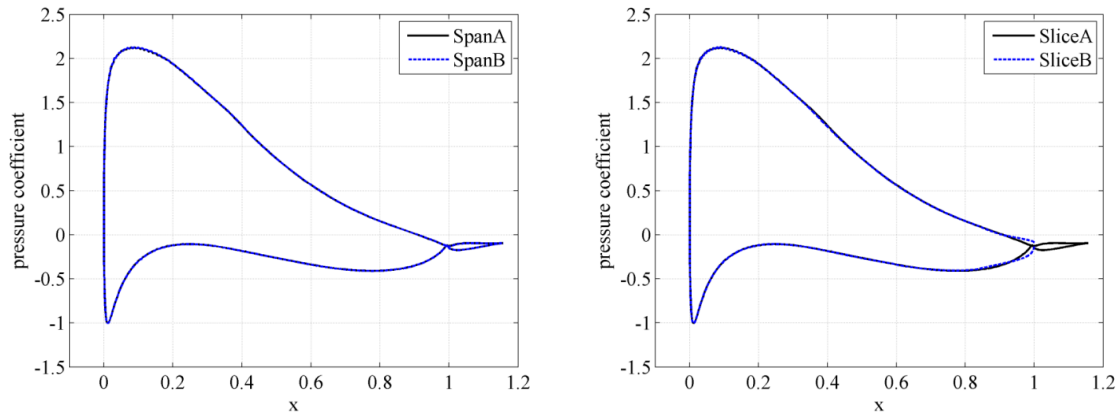

Fig. 4. Cp comparisons with effect of different span size (left) and with a same span size but cut at different spanwise locations (right).

Figures 5 is the stream-wise mean velocity (Fig. 5 (a,c,e)) and stream-wise turbulent stress (Fig. 5 b,d,f). The results are obtained at angles of attack 0, 4 and 8 degrees. The baseline airfoil is used as reference to compare with serrated airfoils. Along the airfoil span positions, it can be seen that the mean velocity profile is overlapped with each other for all three angles of attack as expected. The increase of boundary layer thickness is also observed while angle attack increases. The fluctuating part, such as the turbulent stresses, have some small variation in amplitude. The sound pressure level of the baseline airfoil is shown in Fig. 6. The noise level is increasing as angle of attack changes from 0 to 8 degrees. At higher angle of attack, the larger scale fluctuation also creates higher low frequency noise, as seen from Fig.6. Fig. 7 is the flow results obtained from airfoils with TES. The caption of Fig. 7 'λ/L0.5-β0-L/c14-0/4/8AoA' has the following the meaning: 'λ/L0.5' means wavelength to amplitude ratio is 0.5, 'β0' means zero TE flap angle, 'L/c14' means amplitude to airfoil chord ratio is 14%, '0/4/8AoA' means for all three angles of attack. The results obtained from boundary layer flow clearly show some differences from the case with original airfoil, especially the turbulent stress. The tendency of the boundary layer thickness is found such that the the thickness is smaller in the middle of the serration. The increase of angle of attack always leads to increase of boundary layer thickness which is the same as baseline airfoil. The sound pressure level is reduced by introducing the TES. Fig. 8 shows the spectra at three angles of attack. More noise reduction is seen towards low frequency part, where almost 10dB reduction is seen at 500Hz with angle of attack 8 degrees. Fig. 9 shows similar results as Fig.8, but with a smaller wavelength. With a smaller wavelength of the TES, the noise level is slightly increased. Again, Fig. 10 obtains similar results as Fig. 8, but with an increased flap angle of β5. It is seen that there is a little noise reduction for the case of zero AoA, there is no significant change for other AoAs. Fig. 11 shows the relative noise reduction as compared with the baseline airfoil. In general, it shows that when angle of attack is increased, less overall reduction is achieved for the present TES configuration.
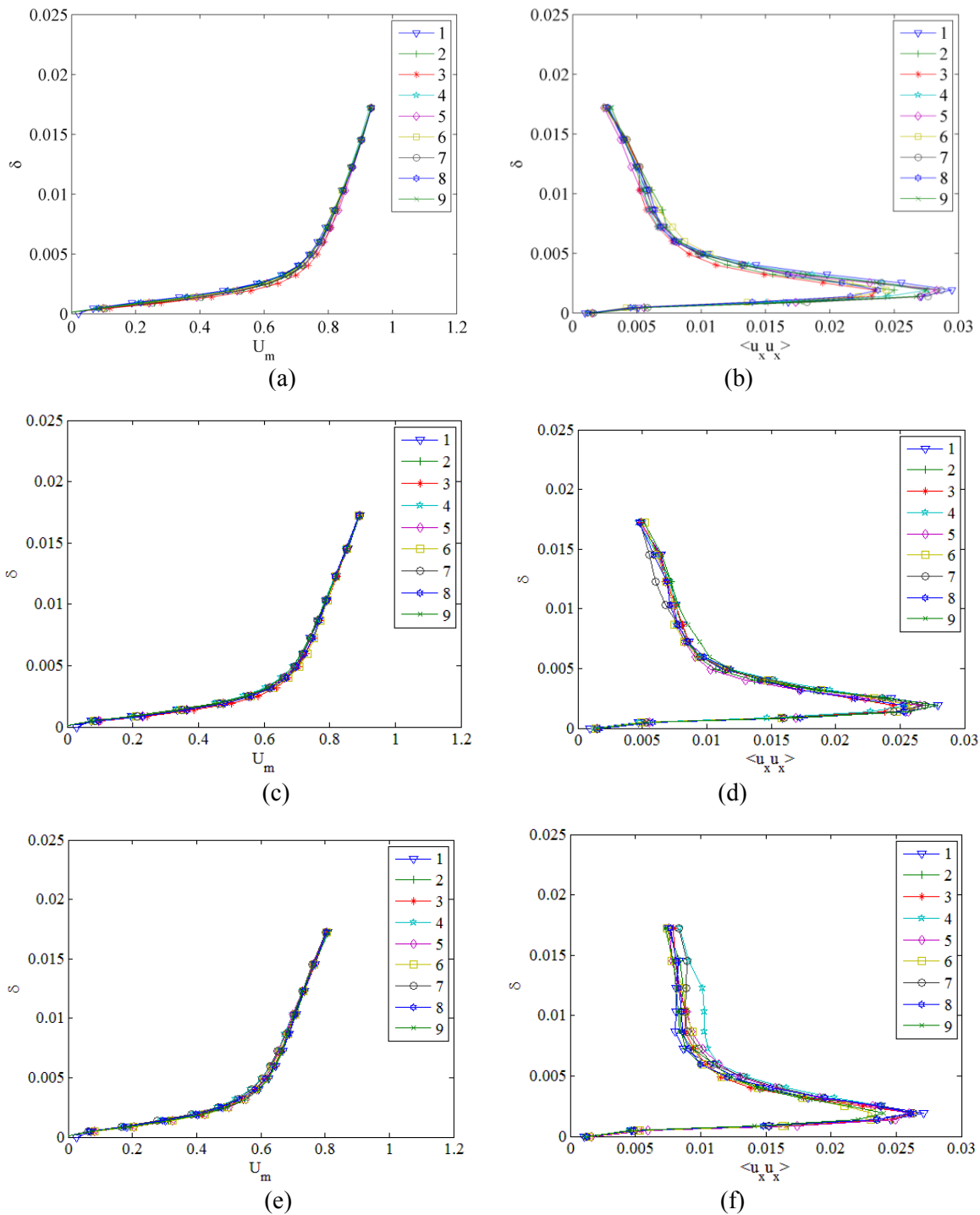
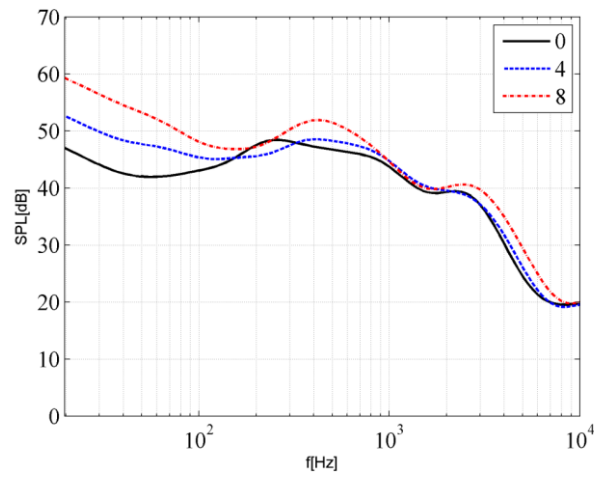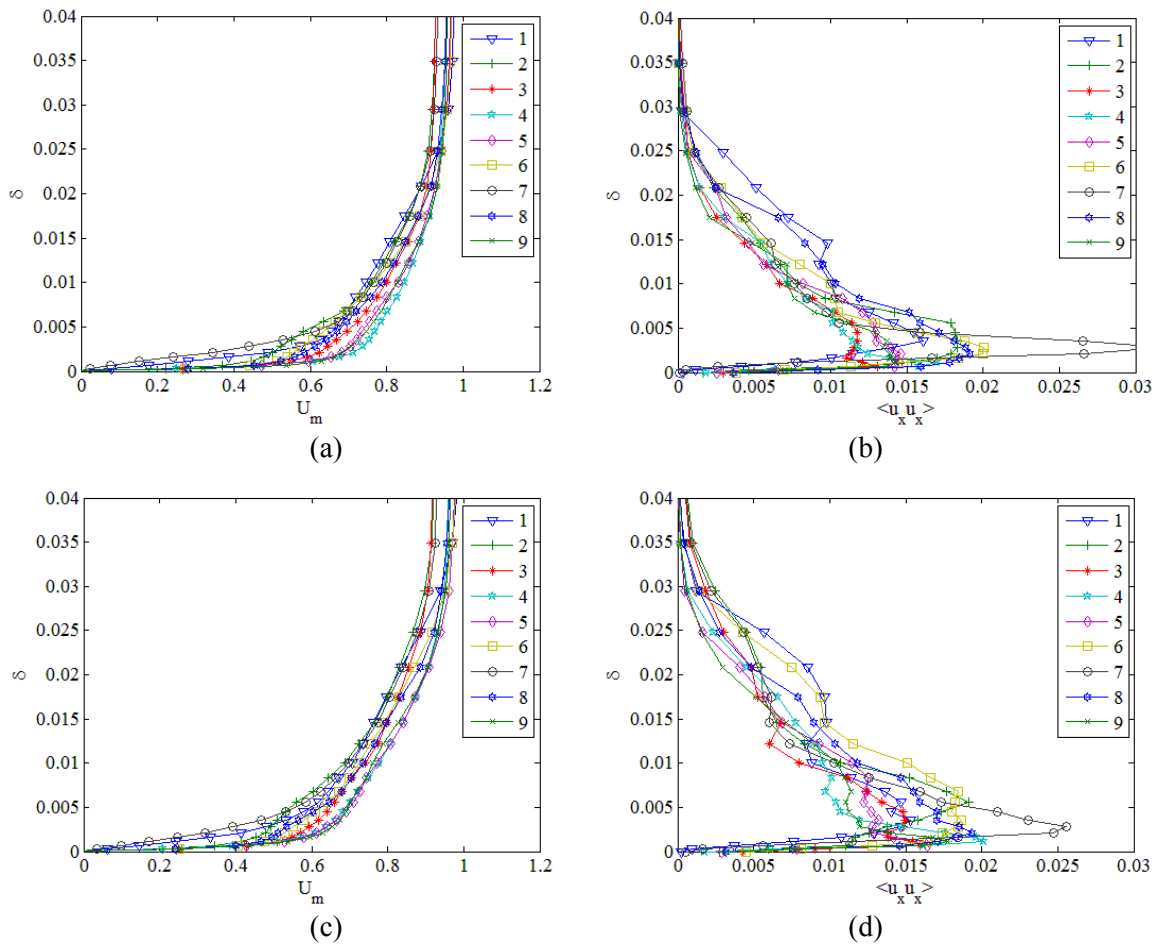Fig. 5 Non-dimensional flow results: Original airfoil. 0/4/8 degrees

Fig. 6 Acoustic results: Original airfoil. 0/4/8 degrees

(a)

(b)

(c)
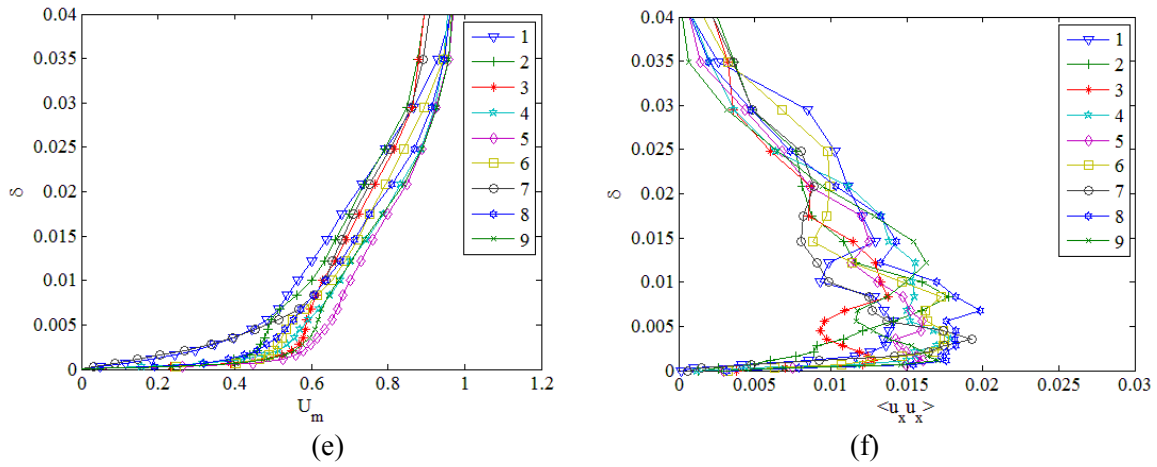

(d)

(e)   (f)

Fig. 7 Non-dimensional flow results: λ/L0.5-β0-L/c14-0/4/8AoA
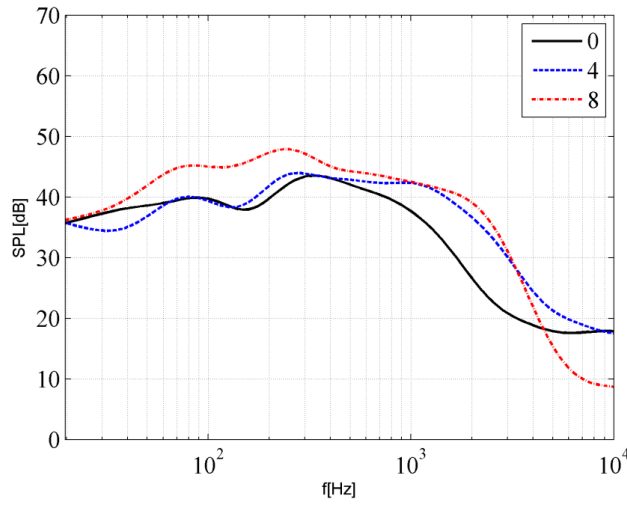
Fig. 8 Acoustic results: λ/L0.5-β0-L/c14
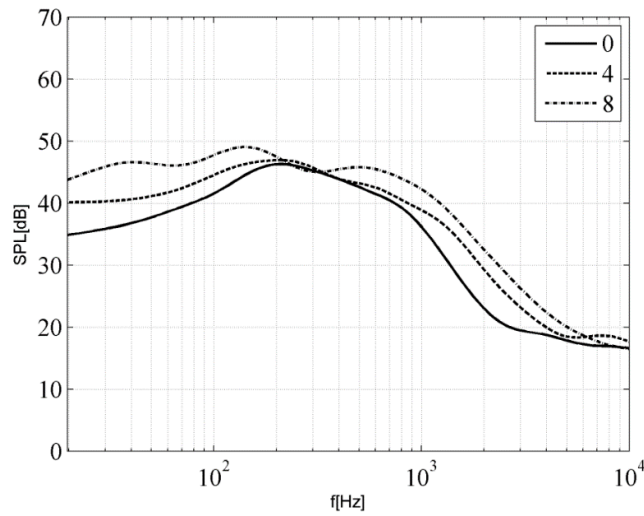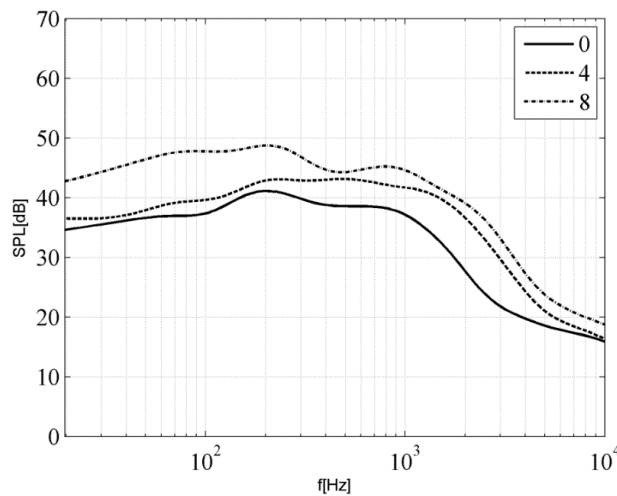

Fig. 9 Acoustic results: λ/L0.25-β0-L/c21
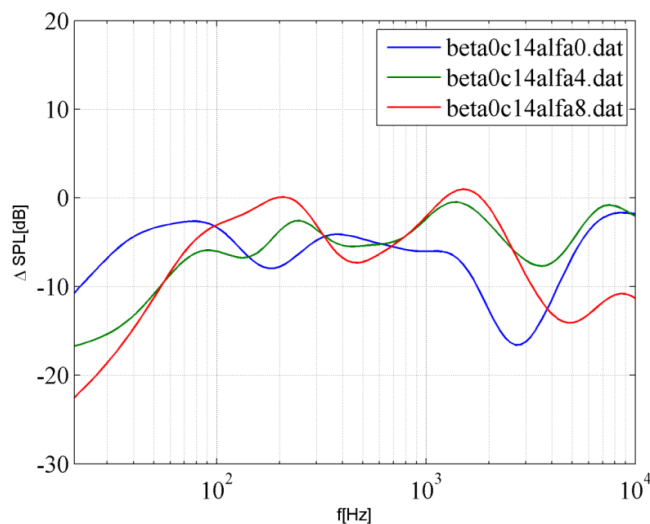
Fig. 10 Acoustic results: λ/L0.5-β5-L/c14

Fig. 11 Relative noise reduction.

4. Conclusions

During the parametric study of the TES, it is found that the noise level of the current airfoil is reduced nearly in all the configurations over a large range of frequency. It is observed that when the 'L/c' ratio increases, the change of the turbulent stress is large which indicates stronger spanwise variation. The present airfoil is a non-symmetric wind turbine airfoil, the change of TE flap angle from -5 to 5 degrees gives quite significant difference at the trailing edge flow. The case with β=-5° gives more 3D effects along the spanwise direction where the difference of the mean velocity and the turbulent stress is much larger along the span. The combination of 'λ/L, β, L/c, α' becomes four-dimensional which makes the conclusion more difficult. The general tendency is that a smaller wavenumber to amplitude ratio (λ/L) and negative flap angle give more noise reduction. In terms of reduction as function of frequency, the noise level is most reduced at lower frequency. For different flow angles, the most reduction is found at zero degrees where noise is reduced at frequency around 1kHz-3kHz.

References

[1] Wolf A, Lutz T, Würz W, Krämer E, Stalnov O, Seifert A (2014) *Trailing edge noise reduction of wind turbine blades by active flow control.* Journal of Wind Energy, online: 17 MAR 2014, DOI: 10.1002/we.1737.

[2] Hutcheson F V (2005) *PIV measurements on a blowing flap.* NASA report AIAA 2005-212.

[3] Herr M, Dobrzynski W (2005) *Experimental investigations in low-noise trailing-edge design.* AIAA J. 43(6), 1167-1175.

[4] Finez A, Jondeau E, Roger M, Jacob MC (2010) *Brodband noise reduction with trailing edge brushes.* AIAA paper 2010-3980.

[5] Howe MS (1978) *A review of the theory of trailing edge noise.* J. Sound Vib., 61(3), 437-465.

[6] Howe MS (1991) *Noise produced by a sawtooth trailing edge.* Journal of the Acoustic Society of America, 90(1), 482–487

[7] Braun KA, van der Borg NJCM, Dassen AGM, Doorenspleet F, Gordner A, Ocker J, Parchen R (1999) *Serrated trailing edge noise.* EU Wind Energy Conference.

[8] Chong TP, Joseph PF (2013) *An experimental study of airfoil instability tonal noise with trailing edge serrations.* J. Sound Vib., 332(24): 6335-6358, 2013.

[9] Oerlemans S, Fisher M, Maeder T, Kögler K (2009) *Reduction of wind turbine noise using optimized airfoils and trailing edge serrations.* AIAA J. 47(6), 1470-1481.

[10] Jaworski J W. and Peake N., (2013) *Aerodynamic noise from a poroelastic edge with implications for the silent flight of owls.* J. Fluid Mech. vol. 723, pp. 456-479. doi:10.1017/jfm.2013.139

[11] Bachmann T and Wagner H. (2011) *The three-dimensional shape of serrations at barn owl wings: towards a typical natural serration as a role model for biomimetic applications.* Journal of anatomy , 219(2):192-202. doi: 10.1111/j.1469-7580.2011.01384.x.

[12] Victor F. Kopiev, Mikhail Yu. Zaitsev and Ivan V. Belyaev, (2011) *Noise Reduction Potential through Slat Hook Serrations.* 17th AIAA/CEAS Aeroacoustics Conference(32nd AIAA Aeroacoustics Conference) .

[13] Benyus JM (2002) *Innovation Inspired by Nature.* New York:Perennial.

[14] Farassat F (2007) *Derivation of formulations 1 and 1A of Farassat.* NASA/TM-2007-214853

[15] Michelsen JA (1998) *General Curvilinear Transformation of the Navier-Stokes Equations in a 3D Polar Rotating Frame.* Technical Report AFM 1998-01; Technical University of Denmark.

[16] Sørensen, NN (1995) *General Purpose Flow Solver Applied Over Hills.* RISØ-R-827-(EN) 1995; Risø National Laboratory, Denmark.

[17] Mary I and Sagaut P (2002) *Large eddy simulation of flow around an airfoil near stall.* AIAA J. Vol. 40, No. 6

[18] Zhu WJ, Shen WZ, Bertagnolio F and Sørensen JN (2012) *Comparisons between LES and wind tunnel hot-wire measurements of a NACA 0015 airfoil.* Proceedings of EWEA 2012 - European Wind Energy Conference & Exhibition. European Wind Energy Association (EWEA), 975-982